Chalcogenide Letters

Tech Science Press

http://doi.org/10.32604/cl.2026.088891

REVIEW

Research on Selenide Anode Materials for Alkali Metal Ion Batteries Based on First Principles

Minghui Tan[1,2], Fei Wang[2,*], Shan Yuan[1,2], Xinli Li[1], Jingxia Gao[2], Jinping Zhang[2,*], Yong Zhang[2] and Lei Shi[3]

[1]School of Materials Science and Engineering, Henan University of Science and Technology, Luoyang, China
[2]Faculty of Engineering, Huanghe Science and Technology College, Zhengzhou, China
[3]Henan Zhongfu Industrial Co., Ltd., Gongyi, China
*Corresponding Authors: Fei Wang. Email: wangf157@hhstu.edu.cn; Jinping Zhang. Email: jpzhang@hhstu.edu.cn

Received: 16 July 2026; Accepted: 27 August 2026; Published: 18 September 2026

ABSTRACT: Li/Na/K-ion batteries show huge potential in next-generation energy storage systems, but the limited theoretical capacity of commercial graphite anodes and the relatively large radius of Na/K ions seriously restrict further development, making it urgent to develop new high-performance anode materials. This article begins with the research hotspots of selenide anode materials and systematically reviews the applications of DFT calculations in the field of Li/Na/K-ion battery selenide anodes, covering transition metal dichalcogenides ($MoSe_2$, $TiSe_2$), Janus structures (VSeTe, WSSe), transition metal carboselenides (Zr_2Se_2C, Sc_2Se_2C), multi-anion bridged phosphoselenides ($MoScP_2Se_6$), main-group element layered selenides (Si_2Se_2, $SiSe_2$, β-GeSe, γ-GeSe, β-CSe, GeSeNS, $SnS_{2(1-x)}Se_{2x}$), as well as selenide-based heterostructure composites. Specifically, atomic-scale simulations offer deep insights into how alkali metal ions are adsorbed, their diffusion paths, and the evolution of their electronic structures, providing theoretical guidance for the rational design of high-performance selenide anode materials. And we also systematically compared the theoretical predictions with experimental verification, looked at how the calculated theoretical capacity matched up with the experimental test values and the deviations, analyzed the reasons for those deviations, and summarized the main factors that hinder the experiments. Lastly, this article also looks ahead to the development of simulation studies on selenide anode materials, including using machine learning to speed up material screening, full-cell simulations, studies of multi-ion co-storage mechanisms and so on.

KEYWORDS: First principles; selenide; alkali metal ion battery; anode material

1 Introduction

1.1 Research Background

With the accelerated shift in the global energy structure and the rapid growth of portable electronic devices, electric vehicles, and smart grids, people's demand for efficient and sustainable electrochemical energy storage technology is becoming increasingly urgent [1,2]. Lithium-ion batteries (LIBs), thanks to their high energy density, long cycle life, and good rate performance, have dominated the consumer electronics and electric transportation sectors since they were first commercialized in 1991 [3–5]. However, the limited reserves of lithium and its uneven geographic distribution keep the cost of lithium-ion batteries high, making it difficult to meet the long-term needs of large-scale grid storage and similar applications [6]. Therefore, developing "post-lithium-ion battery" systems based on more abundant elements like sodium and

potassium has become an important research direction in the field of electrochemical energy storage [7–9]. Sodium-ion batteries (SIBs) and potassium-ion batteries (KIBs), because sodium and potassium are abundant, low-cost, and have similar physicochemical properties to lithium, are seen as some of the most promising alternatives to lithium-ion batteries [10–15]. However, Na^+ and K^+ ions are significantly larger than Li^+, which makes it hard for the graphite anodes commonly used in lithium-ion batteries to effectively accommodate the insertion and extraction of sodium and potassium ions [16,17]. As a result, exploring new anode materials that can offer high capacity, fast ion diffusion, and excellent structural stability has become one of the main challenges in advancing sodium/potassium-ion batteries [18–21].

1.2 Status of First-Principles Research on Selenium-Based Anode Materials

Two-dimensional (2D) layered materials have attracted extensive attention as anodes for alkali metal-ion batteries, owing to their high specific surface area, abundant ion adsorption sites, and short ion diffusion paths [22–24]. Among them, transition metal dichalcogenides (TMDs) have become one of the most widely investigated families because of their unique layered structures and tunable electronic properties [25–27]. Within this class, selenium (Se)-based compounds have emerged as particularly promising alternatives to conventional sulfides and oxides. First-principles calculations have revealed that compared to sulfur (S) and oxygen (O), Se possesses a larger atomic radius, higher polarizability, and stronger metallic character, which endow selenides with wider interlayer channels, weaker M–Se bonds, and higher intrinsic conductivity, these properties are inherently favorable for alkali metal ion storage and transport [28]. Fig. 1 summarizes different types of selenides and selenide-based anode materials. In the family of binary TMDs, DFT calculations have been extensively applied to evaluate the structural stability, electronic properties, and ion diffusion behavior of representative selenides such as monolayer $MoSe_2$ and $TiSe_2$ [29]. For Janus structures (VSeTe, WSSe), DFT has revealed the role of intrinsic built-in electric fields arising from asymmetric atomic layers in modulating ion adsorption and diffusion [30]. In emerging TMCCs (Zr_2Se_2C, Sc_2Se_2C) [31], and multi-anion bridged phosphoselenides ($MoScP_2Se_6$), first-principles calculations have been used to assess structural stability, electronic conductivity, and alkali metal ion storage capability. For main-group element layered selenides (including Si_2Se_2, $SiSe_2$, γ-GeSe, β-GeSe, GeSe nanosheets, β-CSe, and $SnS_{2(1-x)}Se_{2x}$), DFT has been employed to predict crystal structures (via CALYPSO), evaluate mechanical properties (e.g., Poisson's ratio), and investigate ion adsorption and diffusion mechanisms. In parallel, selenide-based heterostructures combining selenides with highly conductive materials such as graphene, C_3N, and MXene have also been systematically investigated by DFT, with a focus on interfacial charge redistribution, mechanical reinforcement, and synergistic effects on ion transport.

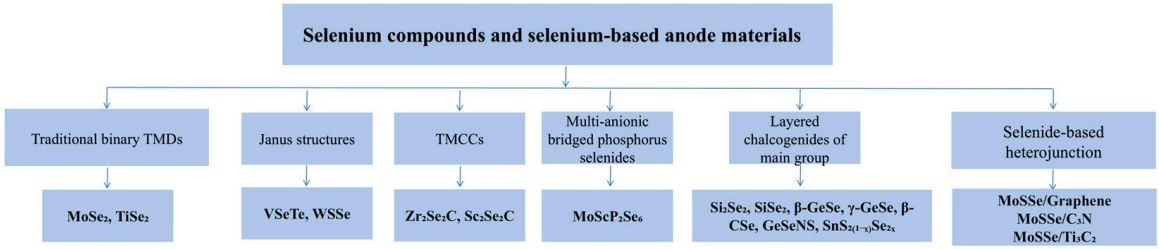

Figure 1: Status of first-principles research on selenium-based anode materials.

1.3 The Key Role of First-Principles Calculations in Studying Anode Materials

1.3.1 The Main Computational Aspects of First-Principles in Anode Materials

First-principles calculations, especially methods based on density functional theory (DFT), have become an essential tool for speeding up the discovery and optimization of battery materials [32–34]. As shown in Fig. 2, the DFT method can accurately predict key material properties at the atomic scale, including crystal structure stability, electronic band structure, ion adsorption energy, diffusion barriers, theoretical capacity, and open-circuit voltage [35,36]. Compared to traditional trial-and-error experiments, theoretical calculations can screen promising candidate materials at lor cost and in less time, and provide clear guidance for experimental synthesis [37].

In the realm of selenide anode materials, DFT calculations have extensively addressed four crucial aspects. Firstly, structural stability is systematically assessed by conducting phonon spectrum calculations to evaluate dynamical stability, binding energy analysis to assess synthetic feasibility, and AIMD simulations to monitor structural evolution at operating temperatures. Secondly, the analysis of electronic structure, encompassing band gap, density of states, and Fermi level position, is conducted to ascertain intrinsic conductivity and reveal the semiconductor-to-metal transition following alkali metal adsorption. Thirdly, ion adsorption and diffusion are quantified through adsorption energy calculations to indicate the strength of ion-substrate interaction, CI-NEB simulations to establish minimum energy pathways and diffusion barriers, and diffusion coefficient evaluation to predict rate performance. Lastly, theoretical capacity and OCV are forecasted through multi-layer adsorption simulations, offering essential parameters for full-cell design. It's generally believed that an anode with a higher OCV is crucial for preventing dendrite growth and keeping the battery safe.

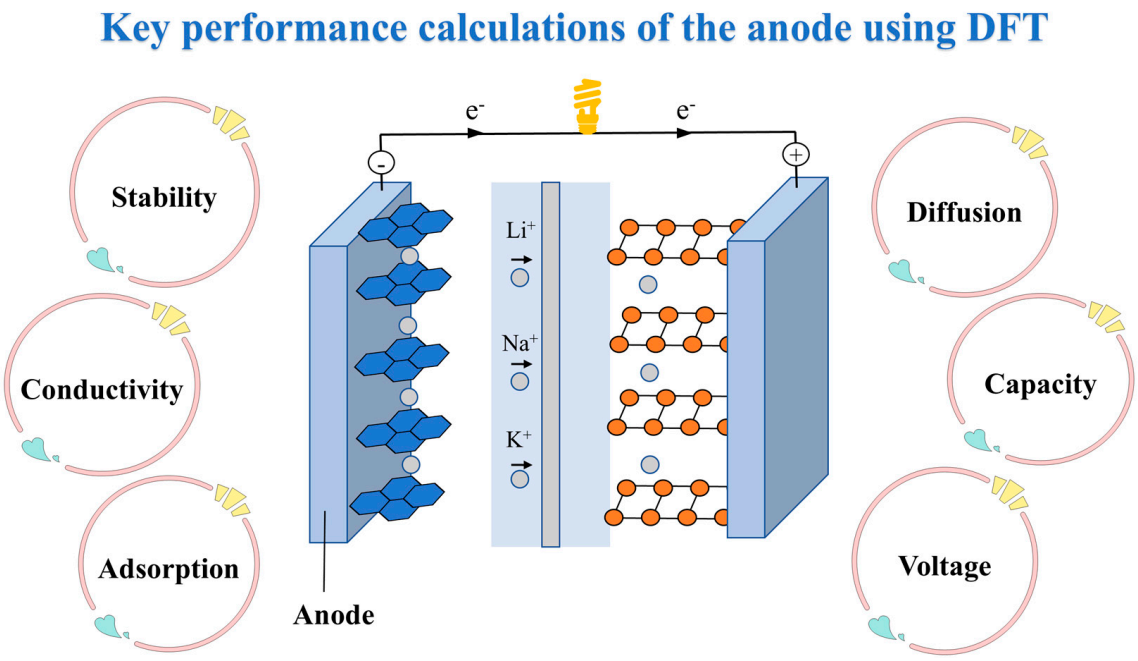

Figure 2: DFT calculations of key performance in ion battery anodes.

1.3.2 The Relationship between DFT Methods and Calculation Results

The theoretical results cited in this review are all based on first-principles calculations under the density functional theory (DFT) framework. We briefly discuss key approximations in DFT methods and

their impact on selenide systems to aid readers in assessing the reliability and comparability of theoretical data. Firstly, the choice of exchange-correlation functional significantly influences computational outcomes. Most studies utilise the Perdew-Burke-Ernzerhof (GGA-PBE) functional within the generalized gradient approximation, which accurately predicts lattice constants, formation energies, and ion adsorption/diffusion trends for selenides. However, it tends to underestimate bandgaps, affecting the understanding of electronic conductivity and charge transfer mechanisms in semiconductor selenides, with PBE-calculated bandgaps typically 30%–50% lower than experimental values. Secondly, van der Waals (vdW) corrections are crucial for layered selenides (e.g., $SnSe_2$, $MoSe_2$). GGA-PBE alone inadequately describes long-range interlayer dispersion interactions, necessitating the introduction of empirical correction schemes like DFT-D3, DFT-D2, or vdW-DF to accurately determine interlayer distances and binding energies. Nevertheless, different vdW correction schemes yield varying results, requiring careful consideration of their specific implementations during comparisons. Thirdly, selenides containing transition metal elements (e.g., $CoSe_2$, $NiSe_2$, $FeSe_2$) may exhibit strong correlation effects of d electrons, potentially causing qualitative inaccuracies in PBE results. In these instances, the DFT+U method may be utilised by introducing a Hubbard U parameter on the d orbitals to enhance electron localisation. However, the selection of U is based on empirical grounds, and variations in U values among different studies directly influence the computed band structures, formation energies, and even voltage profiles. Additionally, hybrid functionals (such as HSE06), which include a specific fraction of Hartree-Fock exact exchange, can notably enhance the precision of bandgap and electronic structure descriptions, particularly beneficial for investigations necessitating accurate assessment of charge transfer properties in semiconductor selenides. Nonetheless, HSE06 entails significantly higher computational costs than GGA-PBE, posing challenges for direct application to extensive supercells or intricate interfaces. Hence, most studies opt for the GGA-PBE+vdW compromise method. Moreover, the configuration of spin polarisation is crucial for magnetic selenide systems with unpaired electrons. The activation of spin polarisation and the selection of spin arrangement (ferromagnetic/antiferromagnetic) can profoundly influence the total energy, magnetic moment, and adsorption energy of the system. Neglecting spin polarisation in certain studies resulted in energy discrepancies of several hundred meV, subsequently impacting assessments of stable configurations.

In summary, differences in theoretical data across studies often stem not only from the materials themselves but also to a significant extent from the choices of computational parameters and approximations mentioned above. When comparing results from different studies, readers should take the consistency of computational methods into account to avoid misinterpreting numerical deviations caused by methodological differences as intrinsic properties of the materials.

1.4 The Purpose and Scope of This Review

In recent years, theoretical research on selenide-based materials for alkali metal ion battery anodes has made significant progress. As an emerging anode material, selenides have been widely studied and shown great potential thanks to their unique layered structure, tunable electronic properties, and relatively high theoretical capacity. Existing review articles have offered valuable summaries on selenide-based anodes, focusing on experimental synthesis routes and electrochemical performance, typically limited to a single alkali metal ion battery system. However, a comprehensive discussion specifically addressing first-principles studies of multicomponent selenides in lithium, sodium, and potassium ion batteries is lacking. This review distinguishes itself by innovating in three key aspects. Firstly, unlike prior works that predominantly summarise experiments, this paper relies on first-principles calculations to present a robust, systematic overview of theoretical advancements concerning selenide anode materials. Secondly, it

surpasses the constraints of a single system by establishing a unified comparative framework encompassing lithium, sodium, and potassium ions, unveiling common physical principles governing the storage and diffusion of various charge carriers in selenides. These principles are often obscured in studies focusing on isolated systems. Thirdly, the scope of our discussion extends from single-component selenides to heterostructured composite materials, conducting a systematic analysis of the structural characteristics, electronic properties, ion storage capacity, and diffusion behaviour of diverse materials. The goal is to help guide the smart design of high-performance selenide anode materials.

1.5 Explanation of Calculable Comparability

The computational results summarised in this review stem from numerous independent DFT studies, each employing distinct calculation parameters. The DFT settings in the cited references exhibit significant variation, encompassing diverse exchange-correlation functionals (e.g., PBE, HSE06, PBE+U), vdW correction methods (such as DFT-D2, DFT-D3, or none), plane-wave cutoff energies (typically 400–600 eV), and k-point sampling schemes. These methodological distinctions have a notable impact on the outcomes. To ensure accurate interpretation of the data in this review, consider the following:

(1) All numerical data (e.g., adsorption energies, diffusion barriers, capacities, and OCV values) are directly extracted from the original authors' reports without recalculation or normalization.
(2) Cross-comparisons between studies are solely employed for trend analysis, not precise benchmarking, due to DFT results' sensitivity to calculation settings. Exercise caution in interpreting side-by-side numerical comparisons.
(3) Future research should adopt consistent computational protocols, incorporating uniform vdW corrections (e.g., DFT-D3 with identical damping parameters), standardised k-point convergence criteria, and, when applicable, uniform treatment of strongly correlated electrons (e.g., DFT+U). This standardisation will significantly enhance the establishment of a comparable database for selenide anode materials, fostering more dependable structure-performance-function relationships.

2 First-Principles Study of Single-Component Selenide Anode Materials

Two-dimensional (2D) selenides have emerged as a prominent focus in research concerning anode materials for alkali metal ion batteries, owing to their distinctive layered structure and tunable electronic properties. Similar to traditional transition metal dichalcogenides, the layers in selenides are held together by weak van der Waals forces, which facilitate natural channels for the insertion and extraction of alkali metal ions. Furthermore, selenium (Se) possesses a larger atomic radius and higher polarizability than sulfur (S) [38,39], resulting in increased spacing between the layers in selenides and reduced energy barriers for ion diffusion. Additionally, compared to M-S bonds, M-Se bonds are weaker, which makes the chemical bonds easier to break and reform during the charging and discharging reactions [40]. This lowers the reaction barriers, helps the reaction kinetics, and promotes full capacity release.

2.1 Transition Metal Selenides

Most transition metal selenides have a hexagonal layered framework structure, where the transition metal atoms coordinate with selenium atoms, forming octahedral or trigonal prismatic configurations, and the layers are held together by van der Waals forces. A few systems, like $MoScP_2Se_6$, use a unique multi-anion bridged structure, its Mo and Sc centers form octahedral coordination with Se and are linked through P_2Se_6 multi-anion units, creating a two-dimensional triangular lattice. The structural diversity and tunable electronic properties of these materials make them one of the most widely studied selenide anode

systems. Table 1 summarizes the key electrochemical performances of various transition metal selenides as anode materials. Based on first-principles calculations, this section systematically reviews the research progress of materials such as $MoSe_2$, $TiSe_2$, Janus 2H-VSeTe, Janus WSSe, Zr_2Se_2C, Sc_2Se_2C, and $MoScP_2Se_6$ as anodes in lithium, sodium, and potassium ion batteries, covering aspects like their structural features, structural stability, conductivity, and electrochemical performance.

Fu et al. [41] studied the Se-Mo-Se three-atom-layer hexagonal structure of monolayer $MoSe_2$ (Fig. 3a) and systematically evaluated its performance as a universal anode for Li/Na/K systems, laying the groundwork for the exploration of future selenide anode materials. Building upon this, Zhao et al. [42] systematically compared the triangular phase structure of monolayer $TiSe_2$ (Fig. 3b) with the lithium storage mechanism of the bulk, revealing how dimensional effects fundamentally impact electrochemical performance and providing an important reference for dimension control in selenide anode materials. The research landscape are further diversified with the emergence of Janus structures. Cao et al. [43] revealed the V-Se/Te sandwich structure of the Janus 2H-VSeTe monolayer material (Fig. 3c) and found that the Se and Te atomic layers form an intrinsic built-in electric field due to significant differences in electronegativity and atomic radius. Similarly, Ahmad et al. [44] systematically studied the S-W-Se sandwich structure of the Janus WSSe monolayer (Fig. 3d), looking into its adsorption and diffusion behavior for Li/Na/K, further improving the understanding of the Janus system in alkali metal ion storage.

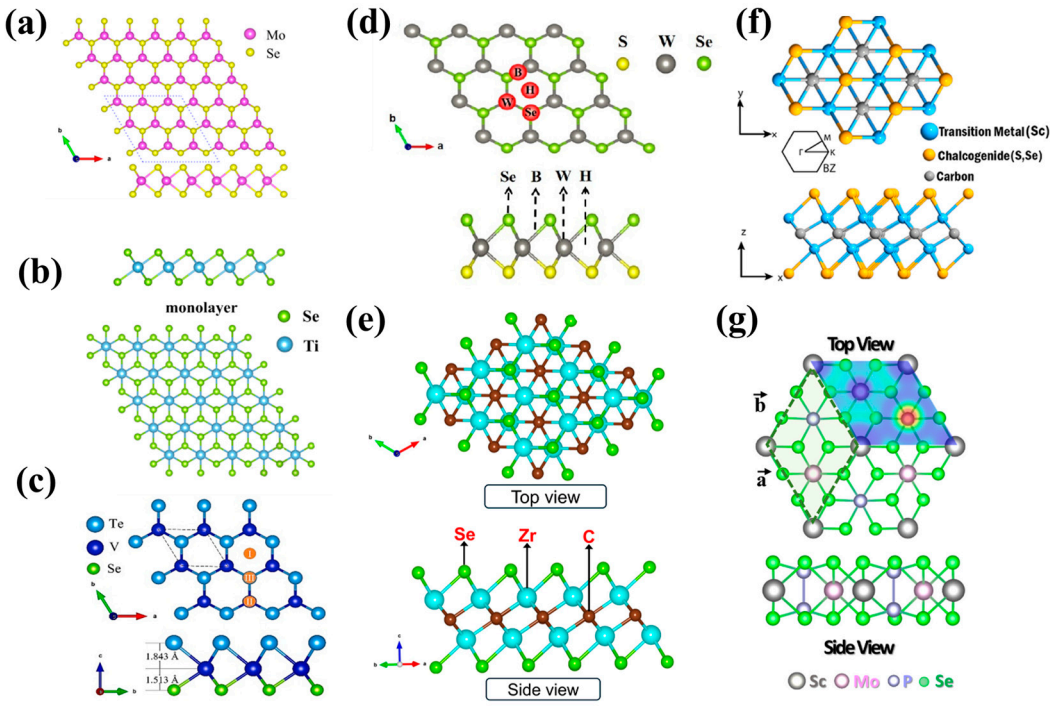

Figure 3: Top view and side view of (**a**) $MoSe_2$, (**b**) $TiSe_2$, (**c**) VSeTe, (**d**) WSSe, (**e**) Zr_2Se_2C, (**f**) Sc_2Se_2C, (**g**) $MoScP_2Se_6$.

In terms of the TMCC family, Martins et al. [45] proposed a layered TMCC structure of Zr_2Se_2C (Fig. 3e) and assessed its potential as a new LIB anode. At the same time, Herabad et al. [46] compared the performance differences of sandwich-type hexagonal lattice structures with S-Sc-C-Sc-S and Se-Sc-C-Sc-Se configurations in Sc_2S_2C and Sc_2Se_2C (Fig. 3f) as Li/Na anodes, further enriching the research on the TMCCs material family. In contrast, Ahmed et al. [47] focused on multi-anion systems, revealing the multi-anion-bridged structure of $MoScP_2Se_6$ (Fig. 3g), where the Mo and Sc centers form octahedral

coordination with Se and are bridged by P_2Se_6 multi-anions to create a 2D triangular lattice, and they demonstrated its potential as a dual-function Na/K anode.

Based on the established structures, researchers further assessed the stability, electronic structure, and diffusion properties of these materials. Fig. 4a shows the phonon spectrum of monolayer $MoSe_2$, with no imaginary frequencies across the entire Brillouin zone, confirming its excellent dynamical stability. This dynamic stability comes from the strong covalent bonding between Mo and Se. Complementary AIMD simulations (Fig. 4b) further demonstrate that the structural integrity of monolayer $MoSe_2$ is well preserved at 300 K, confirming its thermal robustness. Beyond stability, dimensionality effects significantly influence the electrochemical performance of selenides. This is clearly illustrated in Fig. 4c, which compares monolayer and bulk $TiSe_2$. Notably, the monolayer operates via a surface adsorption mechanism, delivering a high capacity of 780 mAh/g within a voltage window of 0.18–1.43 V. In stark contrast, bulk $TiSe_2$ relies on an intercalation mechanism, achieving only 260 mAh/g with a higher voltage plateau of 1.14–2.09 V. This dimension-driven mechanistic shift highlights monolayer engineering as an effective strategy to unlock the intrinsic capacity of selenide materials. The investigation of Janus structures further confirms the importance of thermodynamic stability. For instance, AIMD simulations of Janus 2H-VSeTe (Fig. 4d) reveal no structural distortion within 9 ps at 300 K, confirming its good thermal stability. In addition to stability, the adsorption properties of Janus WSSe were also evaluated. As presented in Fig. 4e, the adsorption energies of Li, Na, and K at the W-top site reach −1.86, −1.19, and −1.03 eV, respectively, demonstrating the strong affinity of WSSe toward alkali metal ions, its a favorable feature for high-performance anode applications.

New types of transition metal carbon chalcogenides (TMCCs) and multi-anion selenides further expand the materials space. Fig. 4f shows the open-circuit voltage curve of Zr_2Se_2C during lithium ion adsorption, and the 0.53 V open-circuit voltage further ensures the safety of Zr_2Se_2C as a lithium-ion battery anode. In terms of electronic conductivity, Fig. 4g presents the band structure of single-layer Sc_2Se_2C, and the fact that it crosses the Fermi level proves that Sc_2Se_2C has good conductivity, which further improves the efficiency of electron transport. Finally, the thermal stability of $MoScP_2Se_6$ was evaluated via AIMD simulations at 300 K over 10 ps (Fig. 4h). The energy fluctuations remain minimal throughout the simulation, and the structure retains its integrity with negligible distortion, demonstrating excellent thermodynamic stability, this is a prerequisite for practical battery operation under varying thermal conditions.

Based on all the calculations and analysis, transition metal selenides show significant advantages in structural diversity, tunable electronic structures, and ion migration properties. Phonon spectra and AIMD simulations both confirm the excellent thermodynamic and kinetic stability of materials like $MoSe_2$, VSeTe, and $MoScP_2Se_6$. Band structure calculations revealed the intrinsic metallic nature of Sc_2Se_2C. The key electrochemical properties of $TiSe_2$, like capacity and open-circuit voltage, show significant differences as the dimensions change. CI-NEB calculations indicate that $MoSe_2$ has the lowest reported Li/Na/K diffusion barrier so far; and adsorption energy calculations confirm the strong affinity of Janus WSSe for alkali metal ions. Overall, monolayer strategies ($TiSe_2$) and Janus structure designs (VSeTe, WSSe) have proven to be effective ways to enhance the electrochemical performance of selenides, while new families like TMCCs (Zr_2Se_2C, Sc_2Se_2C) and multi-anion selenides ($MoScP_2Se_6$) further expand the selection of high-performance anode materials.

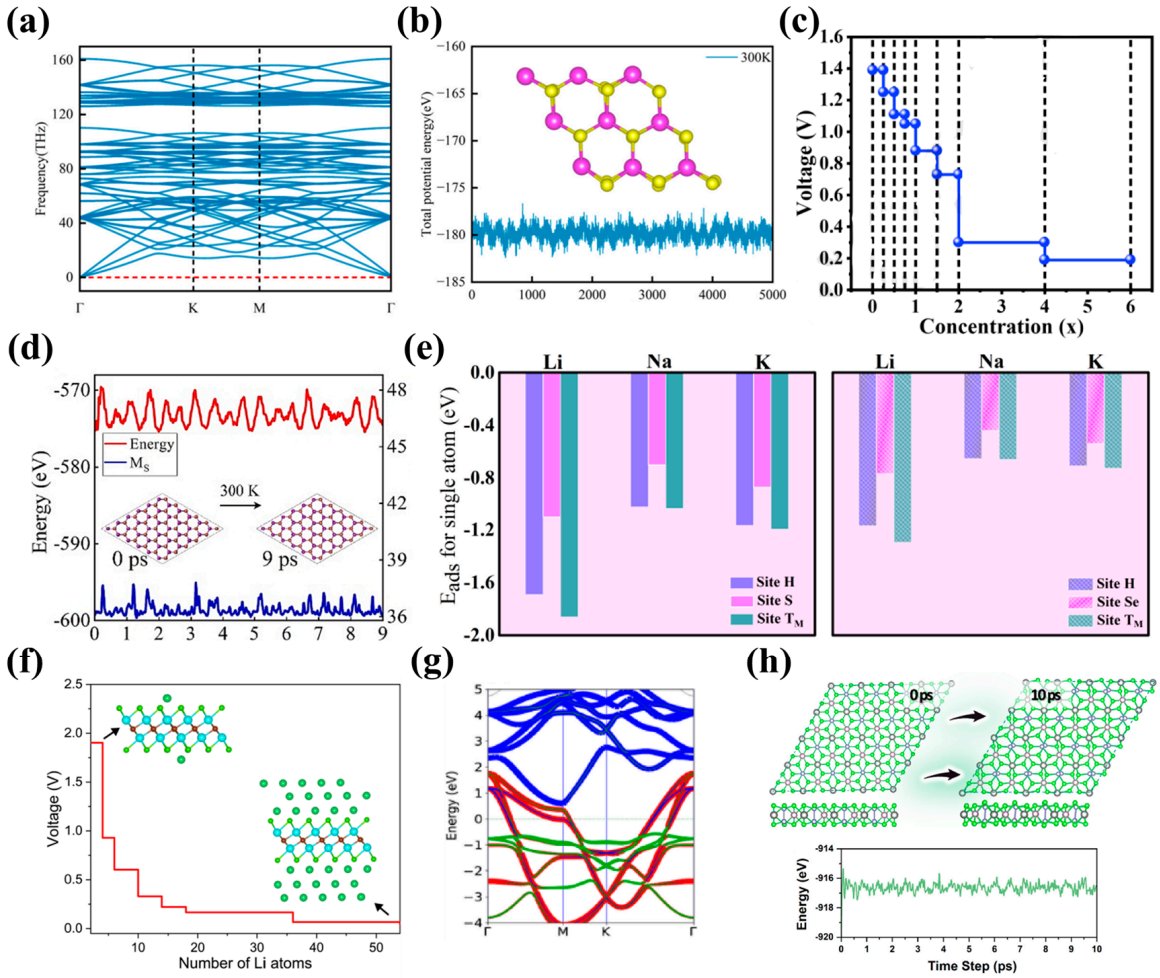

Figure 4: Outstanding properties of transition metal selenides. (**a**) Phonon spectrum of monolayer $MoSe_2$, (**b**) AIMD simulation results of monolayer $MoSe_2$ at 300 K for 5 ps, (**c**) open-circuit voltage of monolayer $TiSe_2$, (**d**) AIMD simulation results of VSeTe at 300 K for 9 ps, (**e**) adsorption energy of Li/Na/K on the W top site in WSSe, (**f**) open-circuit voltage curve of Zr_2Se_2C during lithium ion adsorption, (**g**) band structure curve of monolayer Sc_2Se_2C, (**h**) AIMD simulation results of $MoScP_2Se_6$ at 300 K for 10 ps.

2.2 Main-Group Element Layered Selenides

Unlike transition metal selenides, main group element selenides (like Si, Ge, Sn, C, etc.) have lighter molar masses, which gives them a noticeable advantage in theoretical capacity. These materials also come with a variety of crystal structures, offering plenty of active sites for ion storage. The key electrochemical properties of the main group layered selenides as anode materials are shown in Table 1. Based on first principles, this section systematically introduces the various properties of main-group element selenides like γ-GeSe, β-GeSe, GeSeNS, Si_2Se_2, $SiSe_2$, β-CSe, and $SnS_{2(1-x)}Se_{2x}$, including their material structures, diffusion barriers, and a range of other characteristics.

Moving from transition metal systems to main-group selenides, Shu et al. [48] carried out a systematic theoretical study on γ-GeSe nanosheets. Fig. 5a shows its double-layer honeycomb structure. The study found that the adsorption energy of Li at hollow sites is −1.68 eV, and Bader charge analysis indicates that each Li atom loses 0.89–0.92 e, suggesting strong ionic bonding between Li and the substrate. CI-NEB calculations further revealed that the diffusion barrier of Li along the P1 path is only 0.21 eV. What's

especially noteworthy is that the OCV of γ-GeSe at the maximum lithium adsorption concentration is 0.015, comparable to commercial graphite (0.10 V). In addition to γ-GeSe, other germanium-based selenides have also attracted considerable attention. Zhou et al. [49] studied the β-GeSe monolayer structure (Fig. 5b) and found that its structural symmetry provides ions with isotropic ultrafast diffusion channels. Specifically, the diffusion barriers of Na on the Se side are 0.125 eV and even lower for K at 0.047 eV. These values are among the best reported for 2D anode materials, showing that this material has unique advantages in Na/K ion batteries. Besides germanium-based systems, Zhang et al. [50] reported the puckered honeycomb structure of GeSeNS (Fig. 5c), which is intrinsically a direct bandgap semiconductor. Calculations show that the adsorption energies of Li/Na/K at the most stable adsorption sites are −2.56, −2.04, and −1.41 eV, respectively, all better than the corresponding values for graphene. Besides germanium-based systems, silicon-based selenides have also become strong contenders for high-performance anodes, Wang et al. [51] discovered a new tetragonal phase of Si_2Se_2 (Fig. 5d) through CALYPSO structure prediction. This material is a bilayer nanosheet with a P4/mmm space group, where two buckled SiSe sublayers are linked by Si-Si bonds. The Atop-Si site is the most stable adsorption site (Li −0.67 eV, Na −0.88 eV, K −1.43 eV). Fig. 5d also shows that the diffusion barrier for Li in Si_2Se_2 is only 0.07 eV, which is one of the best values reported among 2D materials. This excellent performance is attributed to the rigid framework provided by the Si-Si bonds and the spacious interlayer channels. As a complementary system to Si_2Se_2, the same study also reported a sandwich structure of $SiSe_2$ (Fig. 5e). The Atop-Se2 site is the most stable adsorption site (Li −0.36 eV, Na −0.30 eV, K −0.67 eV). $SiSe_2$ can reach a capacity of up to 1441 mAh/g for Li, 865 mAh/g for Na, and 180 mAh/g for K. The outstanding performance of silicon-based selenides in capacity makes them strong contenders for high-energy-density anodes. Apart from germanium- and silicon-based materials, Zafer et al. [52] reported the structure of carbon-based selenide β-CSe (Fig. 5f). This material has a Poisson's ratio as low as 0.05 along the armchair direction, which means very little volume expansion when Na is inserted. Fig. 5f also shows that the Na diffusion barrier along the C-side Path 2 in β-CSe is only 0.019 eV, outperforming most reported SIB anode materials.

Table 1: Key performance of single-component sulfide anodes in alkali metal ion batteries.

Material System	Types of Ions	Theoretical Capacity (mAh/g)	Diffusion Barrier (eV)	OCV(V)	References
$MoSe_2$	Li/Na/K	422/422/246	0.036/0.016/0.012	0.66/0.49/0.76	[41]
$TiSe_2$	Li	780	0.039	0.18	[42]
Janus VSeTe	Li	416	0.158	0.638	[43]
Janus WSSe	Li/Na/K	477.8/371.5/156.0	0.18/0.04/0.038	0.48/0.57/0.37	[44]
γ-GeSe	Li	530.36	0.21	0.015	[48]
β-GeSe	Na/K	353.65	0.125/0.047	0.219/0.030	[49]
GeSeNS	Li/Na/K	—	0.329/0.175/0.132	1.82/1.45/1.28	[50]
Si_2Se_2	Li/Na/K	1252/501/250	0.07/0.17/0.17	0.04/0.18/0.06	[51]
$SiSe_2$	Li/Na/K	1441/865/180	0.45/0.43/0.30	0.07/0.04/0.17	[51]
β-CSe	Na	589	0.019	1.11	[52]
Zr_2Se_2C	Li	456	0.20	0.53	[45]
Sc_2Se_2C	Li/Na	403.14	0.20	0.53	[46]
$MoScP_2Se_6$	Na/K	713/687	0.18/0.11	—	[47]
$SnS_{2(1-x)}Se_{2x}$	Li	194	0.37	1.27	[53]

In addition, there has been significant progress in anion engineering of tin chalcogenides. Wang et al. [53] revealed the trade-off between the S/Se ratio in the structure of $SnS_{2(1-x)}Se_{2x}$ alloys and their

performance. Fig. 5g shows that the capacity decreases from 293 to 194 mAh/g as the Se concentration increases, but the OCV remains almost constant (~1.27 V).

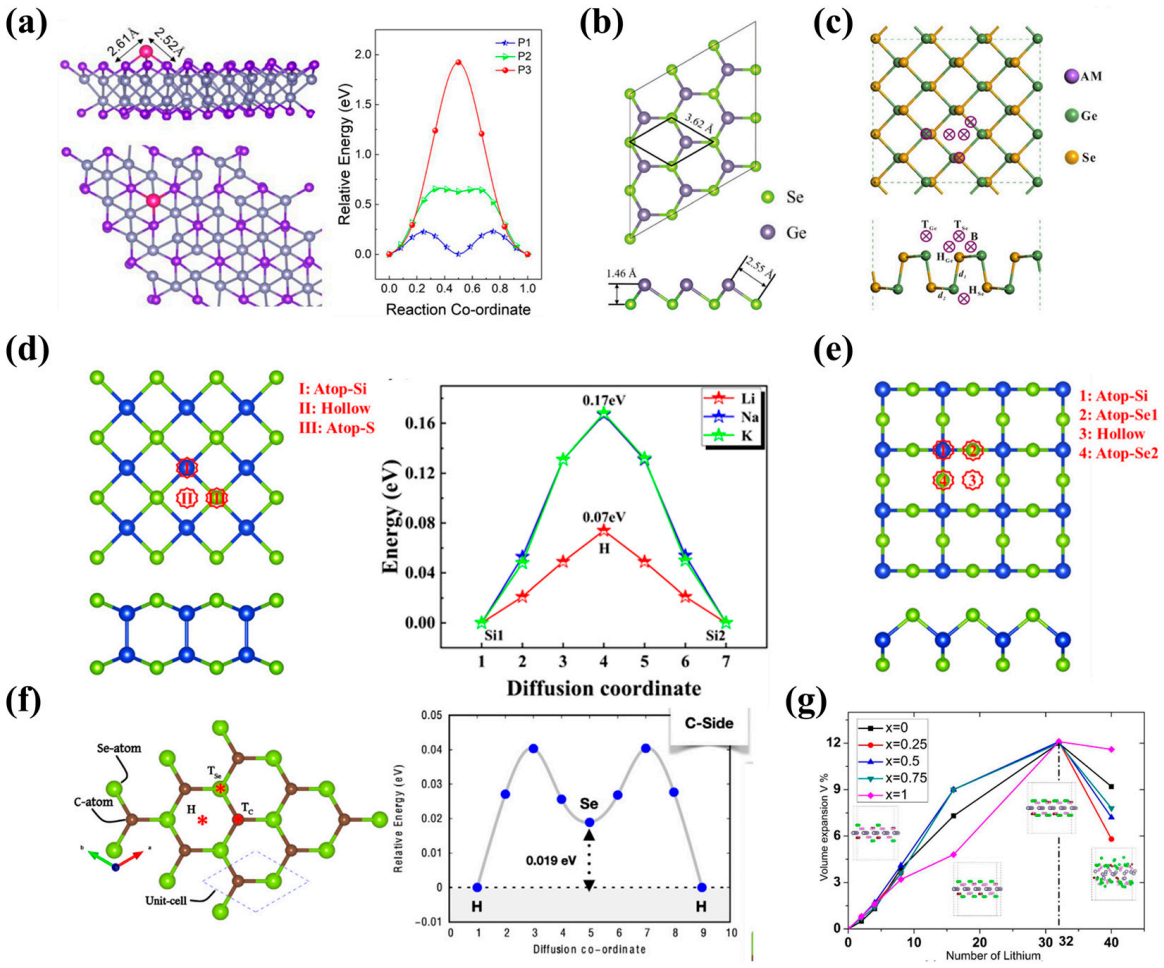

Figure 5: Structure and outstanding properties of layered main group chalcogenides. (**a**) The structure of γ-GeSe and the diffusion energy barrier curve of lithium ions on it, (**b**) monolayer structure of β-GeSe, (**c**) GeSeNS's honeycomb structure, (**d**) the structure of Si_2Se_2 and the diffusion energy barrier curves of Li/Na/K ions on it, (**e**) the sandwich structure of $SiSe_2$, (**f**) the structure of β-CSe and the diffusion energy barrier curve of Na on it, (**g**) change curve of lithium storage capacity with Se concentration.

Based on the calculations and analysis above, main group element layered selenides show significant advantages in theoretical capacity and ion diffusion kinetics. Adsorption energy calculations and Bader charge analysis show that the GeSe series materials (γ-GeSe, β-GeSe, GeSeNS) have a strong affinity for alkali metal ions. Among them, γ-GeSe has an open-circuit voltage (0.015 V) comparable to commercial graphite; the Na and K ion diffusion barriers of β-GeSe are as low as 0.125 eV and 0.047 eV, highlighting its unique advantages for sodium/potassium ion storage. Calculations show that silicon-based selenides (Si_2Se_2, $SiSe_2$) have super high theoretical capacities, with $SiSe_2$ reaching a lithium capacity of 1441 mAh/g. Mechanical property calculations show that β-CSe has a Poisson's ratio of only 0.05 along the armchair direction, and combined with its ultralow Na diffusion barrier of 0.019 eV, this proves its great potential for fast-charging anode applications. The anion alloying strategy ($SnS_{2(1-x)}Se_{2x}$) demonstrates that adjusting the

S/Se ratio can continuously tune the band gap and capacity. Overall, main group selenides have irreplaceable advantages when pursuing extreme capacity (Si-Se systems) and ultrafast ion diffusion (β-CSe).

3 First-Principles Study of Selenium-Based Heterojunction Anode Materials

Although single-component selenides show great potential in terms of capacity and ion mobility, their inherent low conductivity and poor mechanical flexibility seriously limit their practical use. The strategy of building heterostructures combines selenides with a second material that has high conductivity and strong mechanical properties, creating a synergistic enhancement at the interface. The key electrochemical properties of selenium-based heterojunction anode materials as an anode material are shown in Table 2. Based on first principles, this section systematically reviews the various performances of MoSSe/graphene heterojunctions, MoSSe/C_3N heterojunctions, and MoSSe/Ti_3C_2 heterostructures as anodes for alkali metal ion batteries, including their structure, mechanical properties, diffusion barriers, and a range of other properties.

Table 2: Key performance of chalcogenide-based heterojunction anodes in alkali metal ion batteries.

Material System	Types of Ions	Theoretical Capacity (mAh/g)	Diffusion Barrier (eV)	OCV(V)	References
MoSSe/Graphene	Li	560.59	0.17	0.17	[54]
MoSSe/C_3N	Li/Na	494.98/382.08	0.28/0.17	0.17/0.18	[55]
MoSSe/Ti_3C_2	Na	593.3	0.631	0.419	[56]

3.1 Selenide/Carbon-Based Heterojunction

Lin et al. [54] built a MoSSe/graphene heterojunction, and its SeC configuration (Fig. 6a) is one of the best-performing setups. By combining MoSSe with graphene, the lattice mismatch is only 0.70%, and the interlayer spacing is 3.39–3.48 Å. In terms of mechanical performance, the Young's modulus of the heterojunction jumps from 116 N/m for pure MoSSe to 459.3–459.8 N/m, a fourfold increase thanks to the stiff in-plane sp^2-hybridized carbon network of graphene. It performs significantly better in terms of ion storage capacity compared to single-component selenides and graphene. Besides graphene, C_3N is also used to build high-performance heterojunctions. He et al. [55] designed an MoSSe/C_3N heterostructure (Fig. 6b), with a lattice mismatch of only 0.6%. Fig. 6c shows that the diffusion barrier of Li on the S side along Path 1 is 0.28 eV, while for Na on the Se side along Path 1, it drops to 0.17 eV, which is obviously faster than Li. Fig. 6d shows that the OCV of Li for this heterojunction is 0.17 V. The OCV of Na is 0.18V. Considering Na's super-fast diffusion and low OCV, the MoSSe/C_3N heterojunction is particularly suitable for sodium battery systems.

3.2 Selenide/MXene-Based Heterojunction

Zhang et al. [56] combined experiments with DFT calculations to systematically evaluate the sodium storage performance of the MoSSe/Ti_3C_2 heterostructure. Fig. 6e shows the stable adsorption sites of Na between the heterojunction layers, and its adsorption configuration is consistent with the adsorption sites of Na on single components. Fig. 6f shows that the diffusion barrier of Na in MoSSe/Ti_3C_2 heterojunction is 0.631 eV. Electronic structure analysis indicates that MoSSe/Ti_3C_2 has the highest DOS/Fermi level, further proving that forming the heterojunction improves the conductivity of single components.

Based on the calculations and analysis above, selenide-based heterojunctions perform significantly better than single components in terms of mechanical properties, capacity, and conductivity. The Young's

modulus of the MoSSe/graphene heterojunction is about four times higher than that of pure MoSSe (459 N/m), and its capacity is much improved compared to single components. At the heterointerface, the diffusion barrier for Na is generally lower than for Li, with the Na diffusion barrier in MoSSe/C_3N being only 0.17 eV. The theoretical capacity of MoSSe/Ti_3C_2 reaches as high as 593.3 mAh/g. Additionally, the conductivity improves a lot after 'Se connects with MXene' compared to single components. Overall, carbon-based and MXene-based heterojunctions can effectively overcome the intrinsic defects of single selenides through interface synergy.

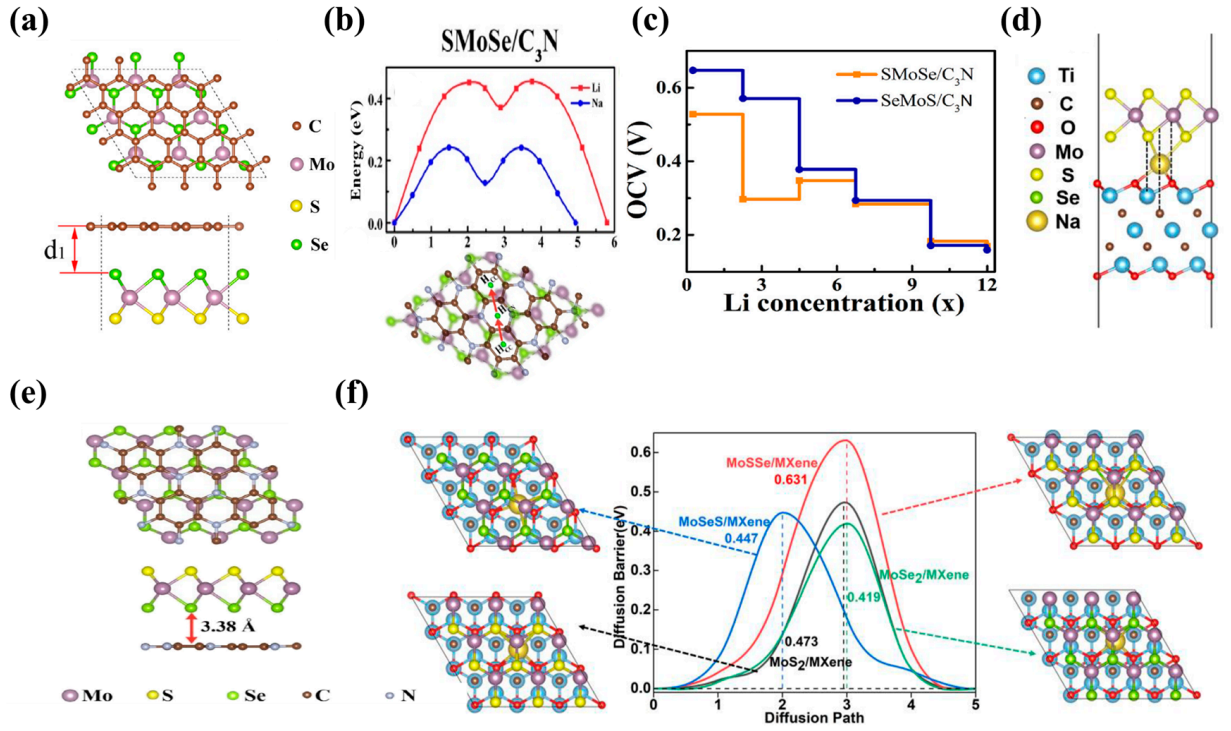

Figure 6: Selenium-based heterojunction structure and outstanding performance. (**a**) The structure of MoSSe/graphene heterojunction, (**b**) the structure of SMoSe/C_3N heterostructure, (**c**) the diffusion barrier curves of lithium/sodium on SMoSe/C_3N heterostructure, (**d**) open-circuit voltage curve of SMoSe/C_3N heterostructure during lithium storage, (**e**) stable adsorption sites of Na between MoSSe/Ti_3C_2 layers, (**f**) Na diffusion energy barrier curve in the MoSSe/Ti_3C_2 heterojunction.

4 Common Microscopic Mechanisms of Alkali Metal Ion Storage in Selenide Anodes

This section steps beyond the limits of specific materials and, from a broader perspective, summarizes the common physical patterns and microscopic mechanisms that selenide anodes show during alkali metal ion storage, including the general evolution of electronic structures, the kinetics of ion adsorption and diffusion, and the underlying design principles for capacity and voltage.

4.1 The Evolution of Electronic Structure

Drawing upon first-principles calculations, this section provides a systematic overview of the electronic structure evolution of selenides and their heterojunction composites upon alkali metal ion adsorption.

Upon the adsorption of alkali metal ions, selenide anode materials generally undergo a semiconductor-to-metal transition, a phenomenon observed in many semiconductor electrode materials. However, what

sets selenides apart from their sulfide and oxide counterparts is not just the occurrence of this transition, but rather its efficiency and extent. This distinction arises from the intrinsic electronic characteristics of selenium (Se). In comparison to sulfur (S) and oxygen (O), selenium exhibits significantly higher polarizability due to its larger atomic radius and more diffuse electron cloud. When alkali metal adsorption takes place, the highly polarizable Se atoms interact more strongly with the injected electrons from the alkali metal ions, thereby facilitating a more efficient electron injection into the conduction band of the host material. This robust orbital hybridization between Se-p and alkali metal-s states leads to a more pronounced and complete semiconductor-to-metal transition. This transition is characterised by a greater reduction in the band gap and a larger increase in the density of states (DOS) at the Fermi level compared to what is typically observed in sulfides or oxides, which have less polarizable anions and wider band gaps. The universality of this phenomenon across various selenide systems further validates the significance of Se's high polarizability. For example, Fig. 7a illustrates that pristine GeSeNS has an intrinsic bandgap of 1.079 eV. Upon the incorporation of alkali metals (Fig. 7b), the electronic states shift to lower energy levels, leading to a distinct semiconductor-to-metal phase transition. Mechanistically, alkali metal atoms significantly impact the Density of States (DOS) near the Fermi level. By populating the conduction band of GeSeNS, these atoms cause the Fermi level to rise, ultimately transitioning the system into a metallic state. A similar transformation occurs in β-CSe. Initially, this material is an intrinsic indirect-bandgap semiconductor with a 1.544 eV gap (Fig. 7c). However, following Na adsorption (Fig. 7d), a finite DOS appears at the Fermi level, signifying a successful shift to a metallic state. This semiconductor-to-metal transition is also evident in Janus structures. For instance, the intrinsic band structure of Janus 2H-VSeTe (Fig. 7e) reveals it as a direct-bandgap semiconductor (0.324 eV). Upon Li adsorption at the V-top site, the material transitions into a metallic state (Fig. 7f). Similarly, Janus WSSe, $SiSe_2$, γ-GeSe and $SnS_{2(1-x)}Se_{2x}$ undergo this transition upon alkali metal ion adsorption. In contrast, selenide systems like $TiSe_2$, Zr_2Se_2C, Sc_2Se_2C, $MoScP_2Se_6$, Si_2Se_2 and so on, which are inherently metallic, either enhance or maintain their metallic properties after alkali metal adsorption, Fig. 8a sums up how well different types of selenides conduct electricity. In these instances, intrinsic metallicity's presence implies that the transition does not shift from a semiconducting to a metallic state but rather strengthens the already existing metallic properties. This reinforcement guarantees consistent high electronic conductivity during charge–discharge cycles.

To summarise, the shift from a semiconductor to a metal prompted by alkali metal adsorption is more prominent in selenide systems than in their sulfide or oxide counterparts. This disparity arises from Se's high polarizability and beneficial orbital hybridization traits. This occurrence secures that electrodes uphold superior electronic conductivity during charge and discharge processes, which is crucial for achieving optimal high-rate performance.

4.2 General Rules of Ion Adsorption and Diffusion Dynamics

This section systematically elucidates, from a first-principles perspective, the adsorption characteristics and diffusion dynamics of alkali metal ions in both pristine selenides and selenide-based heterojunction anodes.

When it comes to adsorption, Bader/Mulliken charge analysis consistently shows that all selenide systems have significant charge transfer of alkali metal ions, which adsorb onto the substrate in ionic form. For example, looking at the charge density difference after Li adsorption on $MoSe_2$ in Fig. 7g, the light green (electron loss) and light pink (electron gain) areas clearly show electrons moving from the Li atom to the neighboring Se atoms. The more charge that gets transferred, the stronger the interaction between the ion and the substrate. As shown in Fig. 8b, we have systematically summarized and compared

the adsorption energies of various selenide materials for alkali metal ions so that readers can easily see the relative performance of different materials in ion adsorption. Generally, the larger the negative value of the adsorption energy, the stronger the bond between the ion and the substrate, and the greater the corresponding charge transfer. This trend is consistent with the results from Bader charge analysis and Mulliken population analysis, confirming the internal consistency of the calculated data. As shown in Fig. 8c, in terms of diffusion dynamics, $MoSe_2$ in single-component selenides exhibits the lowest diffusion barriers, with Li/Na/K being 0.036, 0.016, and 0.012 eV, respectively. This ultra-low barrier comes from the spacious interlayer channels in $MoSe_2$ and the moderate affinity of Se atoms for alkali metal ions. On the other hand, $SiSe_2$ shows the highest diffusion barriers, with Li/Na/K at 0.45, 0.43, and 0.30 eV, mainly because $SiSe_2$ has a dense sandwich structure, so ion migration has to go through a network of Si-Se covalent bonds, making the barrier relatively high. For heterogeneous composite materials, the Li diffusion barriers at the MoSSe/graphene and MoSSe/C_3N heterostructure interfaces are 0.17 eV and 0.28 eV, respectively, which are significantly better than those of single-component materials. This can be attributed to the introduction of graphene and C_3N, which form a charge redistribution layer at the interface, thereby reducing the local interaction barrier between Li and the substrate. In the MoSSe/Ti_3C_2 heterojunction, the diffusion barrier for Na is 0.631 eV, which is relatively high. This is because the MXene surface is rich in functional groups (like -O and -F) that have strong chemical affinity with Na ions, which further increases the migration resistance. Besides, there are various factors impact the determination of adsorption energy and diffusion barriers. Key factors affecting the accuracy of adsorption energy calculations include the selection of the exchange-correlation functional (different functionals may lead to deviations of several eV), the incorporation of van der Waals corrections and the specific schemes used, variations in adsorption configurations, coverage, and supercell sizes (periodic interactions among adsorbates in small supercells can distort outcomes), as well as spin polarization settings (neglecting spin polarization can result in errors of hundreds of meV). Similarly, uncertainties in predicting diffusion barriers mainly arise from the sensitivity of transition state search methods to the initial path (different interpolation methods in the CI-NEB method can cause barrier fluctuations by several times), overestimation of migration barriers due to inadequate supercell size, the impact of van der Waals interactions on diffusion paths in layered systems, and standard DFT calculations disregarding temperature effects (lattice vibrations at the actual operating temperature can significantly diminish the effective barrier). It is important to note that due to the broad range of calculation parameters in different studies, absolute comparisons of adsorption energies and diffusion barriers across literature lack strict significance. Readers should concentrate on relative trends under the same calculation protocol rather than isolated comparisons of absolute values.

In terms of adsorption properties, all alkali metal ions exhibit notable charge transfer in selenide systems. For instance, when $MoSe_2$ adsorbs Li, there is a clear directional movement of electrons from the Li atom to the adjacent Se atom. Concerning diffusion kinetics, within single-component selenides, $MoSe_2$ demonstrates the lowest diffusion barriers (0.036, 0.016, and 0.012 eV for Li, Na, and K, respectively) due to its spacious interlayer channels. Conversely, $SiSe_2$ presents the highest diffusion barriers (0.45, 0.43, and 0.30 eV for Li, Na, and K) because of its dense sandwich structure. In heterojunction composites, the Li diffusion barriers at the MoSSe/graphene and MoSSe/C_3N interfaces are significantly lower, at 0.17 eV and 0.28 eV, respectively, which is due to the reduced migration resistance caused by interfacial charge redistribution. In contrast, Na diffusion in MoSSe/Ti_3C_2 encounters a barrier of 0.631 eV, owing to the strong chemical affinity between the MXene surface functional groups and Na^+. Overall, $MoSe_2$ exhibits superior diffusion performance, thereby enhancing the battery's rate capability.

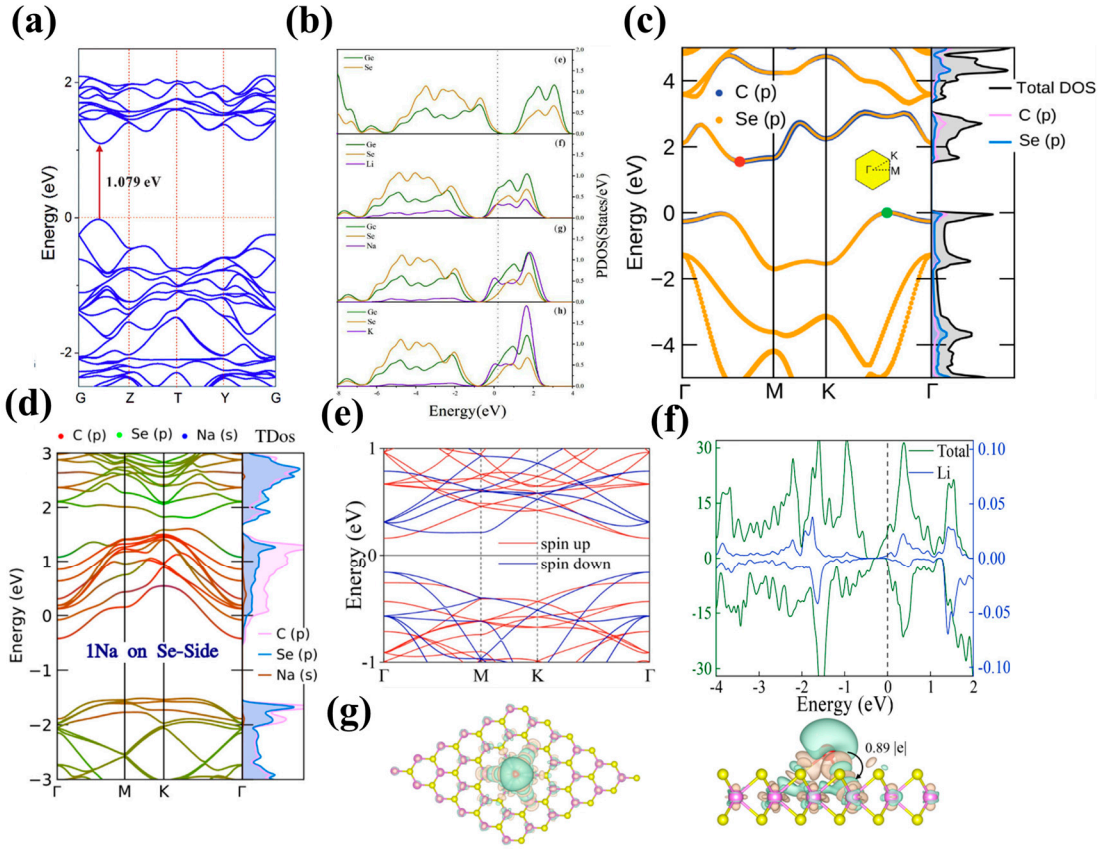

Figure 7: The evolution of the electronic structure of some selenides. (**a**) The band structure of GeSeNS, (**b**) density of states of GeSeNS after adsorbing lithium, sodium, and potassium, (**c**,**d**) intrinsic band structure of β-CSe before and after adsorbing sodium ions, (**e**) intrinsic band structure of VSeTe, (**f**) density of states of VSeTe after adsorbing lithium, (**g**) differential charge density of $MoSe_2$ after Li adsorption.

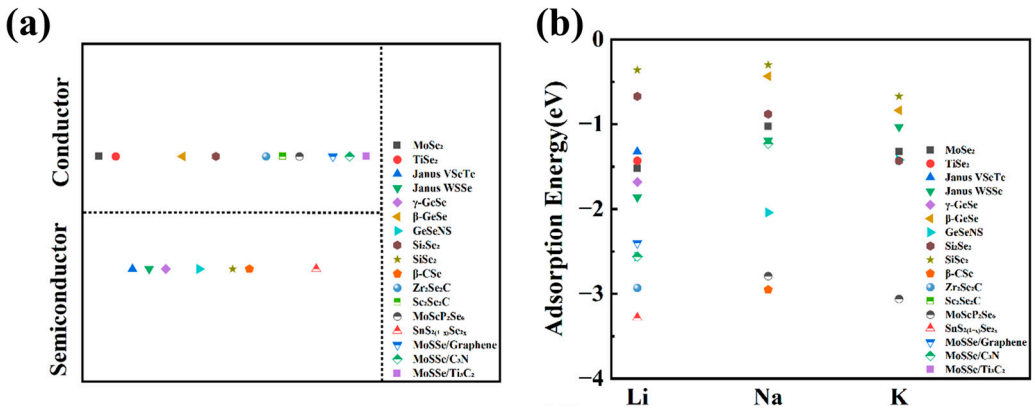

Figure 8: *Cont.*

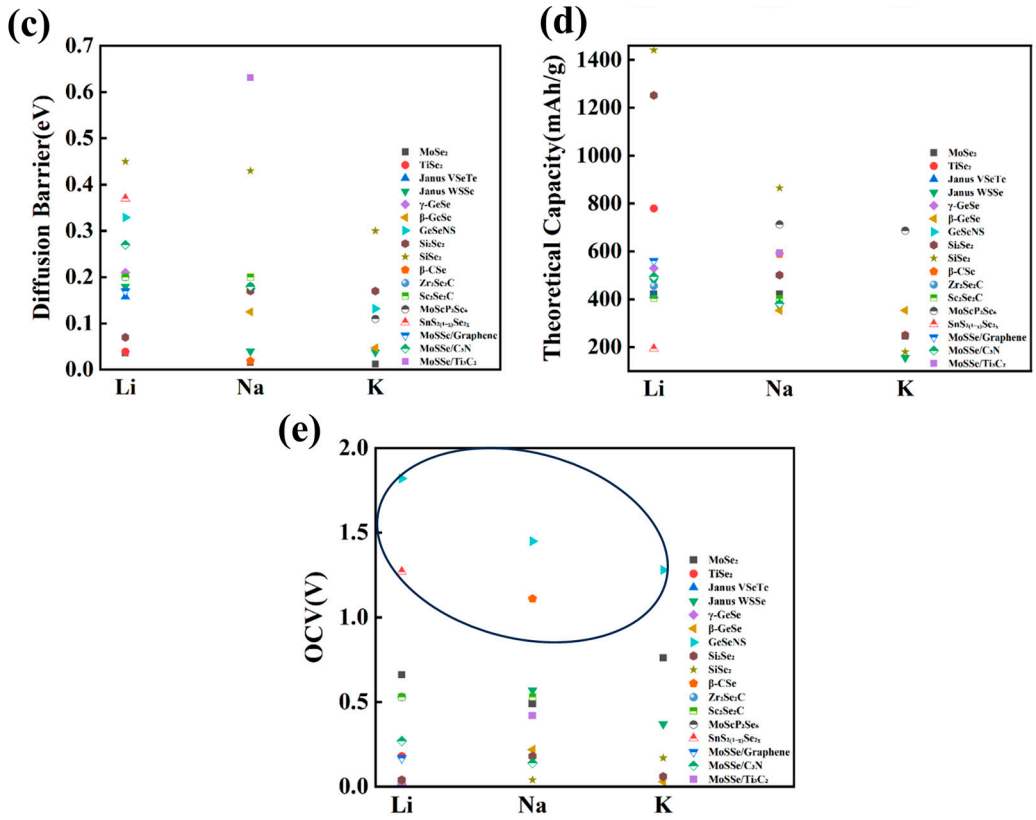

Figure 8: Comparison of intrinsic conductivity (**a**), adsorption energy (**b**), diffusion barriers (**c**), theoretical capacity (**d**) and OCV (**e**).

4.3 Design Principles for Capacity Characteristics and Open-Circuit Voltage

Using first-principles calculations, this section systematically reviews the theoretical capacity and open-circuit voltage behavior of a wide range of selenide materials and their heterojunction counterparts, providing a comparative basis for anode performance evaluation.

The theoretical capacity is the key metric for evaluating the energy storage limit of anode materials. In this article, the selenide materials are organized into two categories: single-component and heterojunction composites. The differences in their capacities reflect the combined effects of the materials' intrinsic properties and structural design. As shown in Fig. 8d, among the single-component selenides, $SiSe_2$ has the highest capacity for lithium and sodium, at 1441 mAh/g and 865 mAh/g, respectively, while $SnS_{2(1-x)}Se_{2x}$ and β-GeSe have the lowest capacities for lithium and sodium, at 194 mAh/g and 353.65 mAh/g, respectively. The reason silicon-based selenides can achieve such ultra-high capacity comes down to two key factors: first, the low molar mass of Si allows more alkali metal ions to be accommodated per unit mass of material; second, this material has multilayer adsorption capability, $SiSe_2$ can adsorb multiple layers, far exceeding the capacity limit of single-layer adsorption. The capacity of $MoScP_2Se_6$ for potassium is up to 687 mAh/g, while WSSe has the lowest at 156 mAh/g. The average capacity for potassium is lower than that for lithium and sodium because potassium ions have a larger ionic radius, so under the same conditions, fewer ions are adsorbed compared to lithium and sodium. In terms of heterojunction composites, $MoSSe/Ti_3C_2$ ranks high with a Na capacity of 593.3 mAh/g. Its capacity advantage comes from the synergistic enhancement at the heterojunction interface: MXene provides a highly conductive framework, while MoSSe contributes high-capacity active sites. Their combination effectively alleviates the capacity limitation of a single

component. The Li capacity of the MoSSe/Graphene heterojunction is 560.59 mAh/g, which also shows the role of carbon-based composites in boosting capacity. Meanwhile, the MoSSe/C_3N heterojunction has capacities of 494.98 and 382.08 mAh/g for Li and Na, respectively, slightly lower than the former two, which might be related to the limited ion storage capacity of C_3N itself. It's worth noting that the capacities of heterojunctions are generally higher than their single selenide components, further confirming the interfacial synergistic enhancement effect. For open-circuit voltage, an ideal anode should have a high and stable voltage plateau. In this study, when using a single selenide material or a selenide heterojunction composite as the anode for alkali metal-ion batteries, the open-circuit voltage generally stays within a reasonable range. As shown in Fig. 8e, only a few materials (GeSeNS, β-CSe, $SnS_{2(1-x)}Se_{2x}$) have open-circuit voltages that fall within the extremely ideal and safe range. Higher open-circuit voltages help suppress dendrite growth, which in turn improves battery safety.

Overall, the silicon-based system ($SiSe_2$) shows the best capacity performance for lithium and sodium (Li 1441 mAh/g, Na 865 mAh/g) thanks to Si's low molar mass and multi-layer adsorption capability. $MoScP_2Se_6$ shows the highest capacity for potassium (K: 687 mAh/g), but in general, potassium's average capacity is lower than that of lithium and sodium due to its larger ionic radius limiting how many ions can be adsorbed. In terms of open-circuit voltage, GeSeNS, β-CSe, and $SnS_{2(1-x)}Se_{2x}$ have relatively high open-circuit voltages, which helps prevent dendrite growth and improve battery safety.

5 Theoretical Predictions and Experimental Verification

This review sums up a lot of theoretical predictions for selenide anode materials based on first-principles calculations, covering key metrics like capacity, voltage, diffusion barriers, and electronic properties. But theoretical predictions only really hold value once they've been verified experimentally. So, in this section, we go through all the materials listed by the reviewers one by one, looking at their experimental synthesis and electrochemical testing status. We clearly separate materials that have documented experimental reports from those that are still purely theoretical predictions, and we dive into comparing DFT predictions with experimental measurements, analyzing any differences and their causes. By systematically comparing theory and experiment like this, we can objectively assess the real-world potential and research maturity of different selenide materials.

After a systematic literature review, among all the selenide-based anode materials covered in this review, some systems have already been experimentally synthesized and their electrochemical properties studied, while others are still at the stage of purely theoretical predictions. Specifically, the selenides that have been experimentally verified and successfully used as battery electrode materials include: $MoSe_2$, $TiSe_2$, GeSe, SnSe, and MoSSe/Ti_3C_2. On the other hand, materials that have not yet been experimentally synthesized and are only predicted based on first-principles calculations include: Janus VSeTe, WSSe, transition metal carboselenides Zr_2Se_2C, Sc_2Se_2C, multi-anion selenide $MoScP_2Se_6$, main-group layered selenides Si_2Se_2, $SiSe_2$, β-CSe, GeSeNS, as well as the heterostructures MoSSe/Graphene and MoSSe/C_3N.

Table 3 summarizes the selenide materials that have been successfully synthesized in experiments and applied as anodes in alkali metal ion batteries, along with their key electrochemical parameters. It should be noted that $TiSe_2$ was tested experimentally in a sodium-ion battery anode system, showing a specific capacity of 283 mAh/g at a current density of 0.1 A/g; in this review, however, the theoretical discussion only considers it as a lithium-ion battery anode. Since these belong to different ion systems, direct comparisons are not made. Regarding the comparison between theoretical and experimental data, the $MoSe_2$ sample had a second discharge capacity of 347 mAh/g, which remained stable for the first 150 cycles, then gradually decreased to 307 mAh/g by the 200th cycle, with a capacity retention of 88.5%. Its experimental capacity

was lower than the DFT-predicted theoretical value of 422 mAh/g. Similar situations are seen with SnSe and MoSSe/Ti_3C_2: SnSe had an initial discharge capacity of 915 mAh/g, with a Coulombic efficiency of 87%, dropping to 184 mAh/g after 100 cycles, a capacity retention of about 20%; MoSSe/Ti_3C_2 showed a capacity of 387.5 mAh/g at 0.1 $A{\cdot}g^{-1}$, and maintained 314.6 mAh/g after 50 cycles at 0.2 $A{\cdot}g^{-1}$. All these experimental values are lower than the DFT predictions, which is because theoretical calculations usually assume ideal crystal structures and fully reversible ion intercalation/deintercalation, while in experiments, irreversible capacity loss mechanisms like SEI formation, structural collapse, and Se dissolution make it hard for the actual capacity to reach the theoretical level. Interestingly, the experimental capacity of GeSe is higher than the DFT-predicted value. Analysis suggests this may be because the GeSe used in experiments was GeSe nanowires prepared via rapid thermal deposition, whereas the GeSe discussed theoretically in this review is β-GeSe and γ-GeSe. These are different crystal structures, and the structural differences account for the gap between experimental capacity and theoretical predictions.

Table 3: Key performance comparison of selenium-based anode materials synthesized through experiments.

Material System	Types of Ions	DFT Predicted Capacity (mAh/g)	Experimental Predicted Capacity (mAh/g)	References
$MoSe_2$	Na	422	347	[57]
$TiSe_2$	Na	/	283	[58]
GeSe	Li/Na	530.36/353.65	815.49/433.4	[59]
SnSe	Li	194	184	[60]
MoSSe/Ti_3C_2	Na	593.3	387.5	[56]

The lack of experimental verification for theoretically predicted materials can be attributed to four main factors. Firstly, Janus structures like VSeTe and WSSe necessitate precise control of the chemical environment on both sides, posing challenges for current experimental methods to achieve atomic-scale selective substitution. Secondly, materials such as Si_2Se_2 and $SiSe_2$ exhibit inadequate structural stability, being susceptible to degradation or oxidation under environmental conditions, thus requiring stringent synthesis and storage conditions. Thirdly, discrepancies between theoretical predictions based on ideal single-layer models in DFT calculations and the practical synthesis of polycrystalline, defect-containing bulk materials hinder direct verification of theoretical hypotheses. Lastly, the electrochemical performance of MoSSe-based heterojunctions, including composites with Graphene or C_3N, is significantly influenced by the stacking arrangement and interface quality, with experimental difficulties in achieving the perfect van der Waals interfaces assumed in theoretical models.

In conclusion, future studies on selenide anodes should advance theoretical innovation through first-principles calculations and refine synthesis methods in line with theoretical projections. Moreover, employing *in-situ* or operando characterisation techniques to track structural changes during charging and discharging in real-time is crucial for bridging the gap between theory and experiment, fostering a symbiotic relationship of ‘theory guiding experiments, and experiments informing theory.

6 Summary and Outlook

Selenides and selenide-based materials, thanks to their excellent electrochemical properties, have become key competitive materials for alkali metal ion batteries. Based on first-principles calculations, this paper systematically reviews the research progress of selenide-based materials as anodes for lithium/sodium/potassium ion batteries.

The review begins with binary transition metal dichalcogenides ($MoSe_2$, $TiSe_2$), expands to Janus structures (VSeTe, WSSe), transition metal carboselenides TMCCs (Zr_2Se_2C, Sc_2Se_2C), multi-anion bridged phosphoselenides ($MoScP_2Se_6$), main-group layered selenides (Si_2Se_2, $SiSe_2$, β-GeSe, γ-GeSe, β-CSe, GeSeNS, $SnS_{2(1-x)}Se_{2x}$), and selenide-based heterojunction composites (MoSSe/Graphene, MoSSe/C_3N, MoSSe/Ti_3C_2). Employing first-principles calculations, the study systematically summarises the research methodologies for assessing material stability, analysing electronic structures, studying ion adsorption and diffusion behaviours, and predicting theoretical capacity and open-circuit voltage. It also utilises computational findings to outline the common microscopic mechanisms of alkali metal ion storage in selenide anodes. Furthermore, a systematic comparison between theoretical predictions and experimental validations is conducted, examining the alignment of calculated theoretical capacities with experimental values, identifying deviations, analysing the causes of these discrepancies, and summarising the primary factors impeding experimental outcomes.

Although first-principles calculations have yielded substantial achievements in the theoretical study of selenide-based anode materials for alkali metal ion batteries, several critical challenges must be overcome to translate theoretical predictions into practical applications. Below, we provide a forward-looking perspective centered on selenide-specific physicochemical issues, complemented by methodological innovations and battery-system expansions: (1) Accurate depiction of van der Waals gaps in selenides is crucial due to their relatively wide interlayer spacing, ranging from approximately 6 Å in $TiSe_2$ to over 8 Å in certain layered configurations, facilitating rapid ion diffusion. Nevertheless, the ability of standard DFT-D3 corrections to fully comprehend the delicate interplay between interlayer expansion upon ion insertion, intercalation energies, and structural stability requires systematic evaluation. Subsequent research should meticulously evaluate state-of-the-art van der Waals-inclusive functionals (such as SCAN-rVV10, optB88-vdW, or many-body dispersion methods) tailored for selenide systems, focusing on $SnSe_2$, $TiSe_2$, and other selenides characterised by extensive interlayer spacings where vdW interactions govern structural stability. This research direction necessitates enhanced computational precision and advocates for the collaborative advancement of multi-scale simulation strategies. These strategies involve using DFT benchmarks to refine machine-learning interatomic potentials, subsequently steering extensive molecular dynamics simulations to explore the prolonged dynamic evolution and phase stability of selenide interlayer configurations. (2) Se vacancy defects and their influence on ion storage and transport in selenide anodes are crucial due to Se's larger ionic radius and higher polarizability compared to S. Se vacancies could lead to distinct defect behaviours, such as the creation of deeper trap states, modification of diffusion pathways, or enhancement of capacity through additional adsorption sites. However, comprehensive Density Functional Theory (DFT) investigations focusing on Se vacancies in selenide anodes are currently scarce. Subsequent research should thoroughly explore the formation energies, migration barriers, and electronic impacts of Se vacancies at different concentrations, along with their combined effects with doping and strain. Special consideration should be given to whether Se vacancies generate extra adsorption sites that boost capacity or modify diffusion pathways in ways that either enhance or impede rate performance. This exploration could potentially introduce novel strategies for defect manipulation in selenide anodes. Methodologically, this research direction would significantly benefit from the advancement of operando theoretical methodologies, utilising constant-potential DFT techniques to model the dynamic behaviour of Se vacancies under practical voltages and their effects on ion intercalation. This approach would effectively connect theoretical forecasts with experimental findings. (3) Composition–performance phase diagram of Se/S anion alloying. Anion alloying, such as $SnS_{2(1-x)}Se_{2x}$, demonstrates potential for tuning electronic structure and capacity. However, a comprehensive computational mapping of composition (x) to key performance metrics—namely band gap, diffusion barrier, theoretical capacity, and open circuit voltage (OCV)—across various host materials (Sn, Ge, Mo, W, etc.) remains absent. Future

research should utilise high-throughput density functional theory (DFT) calculations to systematically construct full composition-range phase diagrams for Se/S alloys within different host systems. Additionally, machine learning-assisted materials discovery can significantly contribute to this effort. By training high-accuracy surrogate models on high-throughput DFT data, it can expedite the exploration of the extensive composition space by several orders of magnitude, while preserving near-DFT prediction accuracy. This approach will facilitate the rapid identification of optimal composition windows to inform experimental synthesis. (4) Theoretical studies on selenide anodes for solid-state batteries aim to address challenges such as selenide dissolution, shuttling effects, and side reactions encountered in traditional liquid systems. Pairing selenide anodes with solid-state electrolytes presents new theoretical inquiries regarding interfacial stability and chemical compatibility between selenides and solid-state electrolytes (e.g., sulfides, oxides, polymers). It also raises questions about whether ion transport kinetics at solid–solid interfaces become a new determining factor in the rate of processes. Additionally, concerns about stress effects resulting from volume changes of selenides under rigid solid-state interfaces during cycling, and the potential for interfacial delamination and battery failure, need thorough investigation. Addressing these queries is crucial through first-principles interface modelling and stress analysis to establish a theoretical basis for engineering the design of solid–solid interfaces. (5) Exploration of selenides in multivalent-ion batteries goes beyond monovalent Li^+, Na^+, and K^+. Multivalent-ion batteries (e.g., Mg^{2+}, Zn^{2+}, Al^{3+}) are gaining attention for their high volumetric capacity and resource abundance. Selenides, with polarizable anionic frameworks and adjustable interlayer spacings, theoretically offer potential for accommodating multivalent ions. However, the stronger electrostatic repulsion between multivalent ions and the host lattice results in higher migration barriers and more complex intercalation/deintercalation pathways. This often involves significant structural reconstruction, making theoretical modeling more challenging. Currently, first-principles studies on multivalent-ion storage in selenides are still in their early stages. Future research should systematically investigate the compatibility of different selenide structure types with $Mg^{2+}/Zn^{2+}/Al^{3+}$, focusing on developing computational models that accurately depict ion–lattice interactions under intense electrostatic environments. (6) AI-driven inverse design of selenide anodes has been predominantly discussed within the context of the forward-design paradigm, which predicts properties from material structures. A more revolutionary approach is AI-powered inverse materials design, which begins with target properties and directly generates candidate selenide structures that meet specific performance criteria using generative models within the material structure space. In the case of selenide anodes, the objective function for inverse design can be defined as a multi-objective optimization that includes high capacity, low voltage hysteresis, rapid ion diffusion, and strong structural stability. Although inverse design is still in its nascent stages and its applications in the selenide field are limited, with the growth of materials databases and the advancement of generative AI models, this direction has the potential to surpass the limitations of traditional trial-and-error methods and emerge as a significant advancement in expediting the discovery of selenide anode materials.

By progressing research in these specific selenide-oriented pathways, selenide-based anodes could transition from theoretical projections to practical implementations, aiding in the development of next-generation secondary batteries characterised by high energy density, superior power output, and cost-effectiveness.

Acknowledgement: The authors thank the Natural Science Foundation of Henan, Zhengzhou Foundation for Basic Research, Postgraduate Education Reform and Quality Improvement Project of Henan Province, the Key Discipline of Henan Province—Materials and Chemical Engineering and Henan Province Science and Technology Research Project to provide project fund support. The authors further thank all individuals who contributed directly or indirectly to this work.

Funding Statement: This research was funded partly by the Natural Science Foundation of Henan, the Zhengzhou Foundation for Basic Research (grant numbers ZZSZX202414 and ZZSZX202412), the Postgraduate Education Reform and Quality Improvement Project of Henan Province (YJS2025GZZ63), the Key Discipline of Henan Province—Materials and Chemical Engineering and Henan Province Science and Technology Research Project (Grant No. 242102231085).

Author Contributions: Study conception and design: Fei Wang, JinPing Zhang, Minghui Tan; data collection: Minghui Tan, Shan Yuan, Xinli Li, Jingxia Gao, Yong Zhang, Lei Shi; analysis and interpretation of results: Minghui Tan; draft manuscript preparation: Minghui Tan; review and editing, Fei Wang, JinPing Zhang. All authors reviewed and approved the final version of the manuscript.

Availability of Data and Materials: The authors confirm that the data supporting the findings of this study are available from the corresponding authors upon reasonable request.

Ethics Approval: Not applicable.

Conflicts of Interest: The authors declare that they have no known competing financial interests or personal relationships that could have appeared to influence the work reported in this paper. Given his role as EB of this journal, [Fei Wang] had no involvement in the peer review of this article and had no access to information regarding its peer review. Full responsibility for the editorial process for this article was delegated to another journal editor. The authors declare no conflicts of interest.

References

1. Wang S, Jiao S, Tian D, Chen HS, Jiao H, Tu J, et al. A novel ultrafast rechargeable multi-ions battery. Adv Mater. 2017;29(16):1606349. [CrossRef].
2. Liu Q, Wang H, Jiang C, Tang Y. Multi-ion strategies towards emerging rechargeable batteries with high performance. Energy Storage Mater. 2019;23:566–86. [CrossRef].
3. Xie J, Lu YC. A retrospective on lithium-ion batteries. Nat Commun. 2020;11:2499. [CrossRef].
4. Megahed S, Scrosati B. Lithium-ion rechargeable batteries. J Power Sources. 1994;51(1–2):79–104. [CrossRef].
5. Horiba T. Lithium-ion battery systems. Proc IEEE. 2014;102(6):939–50. [CrossRef].
6. Rajput K, Kumar V, Thomas S, Zaeem MA, Roy DR. Ca_2C MXene monolayer as a superior anode for metal-ion batteries. 2D Mater. 2021;8(3):035015. [CrossRef].
7. Gao Y, Zhang H, Peng J, Li L, Xiao Y, Li L, et al. A 30-year overview of sodium-ion batteries. Carbon Energy. 2024;6(6):e464. [CrossRef].
8. Li X, Guo S, Qiu F, Wang L, Ishida M, Zhou H. $Na_2Ru_{1-x}Mn_xO_3$ as the cathode for sodium-ion batteries. J Mater Chem A. 2019;7(9):4395–9. [CrossRef].
9. Ji B, Zhang F, Song X, Tang Y. A novel potassium-ion-based dual-ion battery. Adv Mater. 2017;29(19):1700519. [CrossRef].
10. Su H, Jaffer S, Yu H. Transition metal oxides for sodium-ion batteries. Energy Storage Mater. 2016;5:116–31. [CrossRef].
11. Zhao Q, Whittaker AK, Zhao XS. Polymer electrode materials for sodium-ion batteries. Materials. 2018;11(12):2567. [CrossRef].
12. Xia Q, Li W, Miao Z, Chou S, Liu H. Phosphorus and phosphide nanomaterials for sodium-ion batteries. Nano Res. 2017;10(12):4055–81. [CrossRef].
13. Hosaka T, Shimamura T, Kubota K, Komaba S. Polyanionic compounds for potassium-ion batteries. Chem Rec. 2019;19(4):735–45. [CrossRef].
14. Zhou M, Bai P, Ji X, Yang J, Wang C, Xu Y. Electrolytes and interphases in potassium ion batteries. Adv Mater. 2021;33(7):2003741. [CrossRef].
15. Zhang W, Huang W, Zhang Q. Organic materials as electrodes in potassium-ion batteries. Chem A Eur J. 2021;27(20):6131–44. [CrossRef].
16. Gao L, Zeng J, Ge X, Gao T, Wang Y, Sun Z, et al. Biomass-derived carbon with heavy doping for anode of potassium ion batteries. Adv Mater. 2026;38(12):e20046. [CrossRef].

17. Heyns R, Markowski R, Kachmar A, Ingenmey J, Monnens W, Vlad A, et al. Cyclic ether-based electrolyte solutions for potassium metal batteries. Energy Adv. 2026;5(7):947–59. [CrossRef].
18. Tesfaye AT, Mashtalir O, Naguib M, Barsoum MW, Gogotsi Y, Djenizian T. Anodized Ti $_3$ SiC $_2$ as an anode material for Li-ion microbatteries. ACS Appl Mater Interfaces. 2016;8(26):16670–6. [CrossRef].
19. Jiang N, Li B, Ning F, Xia D. All boron-based 2D material as anode material in Li-ion batteries. J Energy Chem. 2018;27(6):1651–4. [CrossRef].
20. Chang YM, Lin HW, Li LJ, Chen HY. Two-dimensional materials as anodes for sodium-ion batteries. Mater Today Adv. 2020;6:100054. [CrossRef].
21. Zhang J, Liu G, Hu H, Wu L, Wang Q, Xin X, et al. Graphene-like carbon-nitrogen materials as anode materials for Li-ion and mg-ion batteries. Appl Surf Sci. 2019;487:1026–32. [CrossRef].
22. Kim HG, Lee HBR. Atomic layer deposition on 2D materials. Chem Mater. 2017;29(9):3809–26. [CrossRef].
23. Zhang Y, Liu Q, Zhang D, Hong Y, Li Q. Anisotropic etching of 2D layered materials. ChemPhysMater. 2024;3(4):341–56. [CrossRef].
24. Stark MS, Kuntz KL, Martens SJ, Warren SC. Intercalation of layered materials from bulk to 2D. Adv Mater. 2019;31(27):1808213. [CrossRef].
25. An Y, Hou Y, Wang K, Gong S, Ma C, Zhao C, et al. Multifunctional lateral transition-metal disulfides heterojunctions. Adv Funct Mater. 2020;30(32):2002939. [CrossRef].
26. Schulman DS, May-Rawding D, Zhang F, Buzzell D, Alem N, Das S. Superior electro-oxidation and corrosion resistance of monolayer transition metal disulfides. ACS Appl Mater Interfaces. 2018;10(4):4285–94. [CrossRef].
27. Huang Z, Jia J, Liu X, Li J, Guo Y, Liang H. Volcano plot of transition metal disulfides in aqueous zinc ion storage. Nano Lett. 2026;26(19):6379–85. [CrossRef].
28. Wang J, Sun Z, Wang K, Wang Y, Liu F, Liao J, et al. Microstructure design of metal selenides for sodium-ion battery anodes. Small. 2025;21(42):e06739. [CrossRef].
29. Yang R, Ye H, Zhu D, Sun Y, Wang Q, Liu Y, et al. Controlling spontaneously-formed nanoscrolls by in-plane Janus TMD/traditional TMD heterostructures. ACS Appl Mater Interfaces. 2026;18(4):7258–68. [CrossRef].
30. Hong H, Wang Y, Wei Z, Yang X, Wu Z, Guo X, et al. Constructing a Janus catholyte/cathode structure: A new strategy for stable Zn-organic batteries. Adv Mater. 2024;36(46):2410209. [CrossRef].
31. Majed A, Kothakonda M, Wang F, Tseng EN, Prenger K, Zhang X, et al. Transition metal carbo-chalcogenide "TMCC:" a new family of 2D materials (adv. mater. 26/2022). Adv Mater. 2022;34(26):2270198. [CrossRef].
32. Clark SJ, Segall MD, Pickard CJ, Hasnip PJ, Probert MIJ, Refson K, et al. First principles methods using CASTEP. Z Für Kristallogr Cryst Mater. 2005;220(5–6):567–70. [CrossRef].
33. Perdew JP, Burke K, Ernzerhof M. Generalized gradient approximation made simple. Phys Rev Lett. 1996;77(18):3865–8. [CrossRef].
34. Perdew JP, Chevary JA, Vosko SH, Jackson KA, Pederson MR, Singh DJ, et al. Atoms, molecules, solids, and surfaces: Applications of the generalized gradient approximation for exchange and correlation. Phys Rev B. 1992;46(11):6671–87. [CrossRef].
35. Tan M, Zhang J, Yuan S, Wang F, Li X, Shi L. Bi-functionalized MXenes(Ti_2CBi_2/Sc_2CBi_2) as electrode materials for alkali metal (Li, Na, K) ion batteries: A DFT study. Int J Hydrogen Energy. 2026;227:154530. [CrossRef].
36. Tan M, Zhang J, Yuan S, Wang F, Li X, Shi L. Bi-modified V_2C MXene (V_2CBi_2) monolayer film as an anode for alkali metal-ion (Li/Na) batteries: A first-principles study. New J Chem. 2026;50(24):10087–100. [CrossRef].
37. Akbar M, Ain NU, Khan MI, Alotaibi R, Ali SM, Ashraf N. A DFT study of monolayer magnesium carbide (MgC_2) as a potential anode for (Li, Na, K) alkali metal-ion batteries. Phys Chem Chem Phys. 2025;27(13):6570–82. [CrossRef].
38. Choi I, Ha S, Kim KH. Review and recent advances in metal compounds as potential high-performance anodes for sodium ion batteries. Energies. 2024;17(11):2646. [CrossRef].
39. Panigrahi R, Mallik BS. Chalcogen effects and cathodic properties of scandium-based materials for sodium-ion batteries. Ionics. 2024;30(8):4665–74. [CrossRef].
40. Huang YX, Wu F, Chen RJ. Thermodynamic analysis and kinetic optimization of high-energy batteries based on multi-electron reactions. Natl Sci Rev. 2020;7(8):1367–86. [CrossRef].

41. Fu X, Zhang X, He X, He Z, Ma L, Wang H, et al. First-principles design of high-performance monolayer $MoSe_2$ anode for multiple ions batteries. J Power Sources. 2026;667:239218. [CrossRef].
42. Zhao C, Wang D, Lian R, Kan D, Dou Y, Wang C, et al. Revealing the distinct electrochemical properties of $TiSe_2$ monolayer and bulk counterpart in Li-ion batteries by first-principles calculations. Appl Surf Sci. 2021;540:148314. [CrossRef].
43. Cao Z, An Y. Explore the feasibility of Janus 2H-VSeTe monolayer as anode material for Li ion battery. J Electroanal Chem. 2023;947:117786. [CrossRef].
44. Ahmad S, Din HU, Nawaz S, Nguyen ST, Nguyen CQ, Nguyen CV. First principles study of the adsorption of alkali metal ions (Li, Na, and K) on Janus WSSe monolayer for rechargeable metal-ion batteries. Appl Surf Sci. 2023;632:157545. [CrossRef].
45. Martins NF, Gonzalo FM, Laranjeira JAS, Rivera VJR, Denis PA, Sambrano JR. First-principles investigation of metallic Zr_2Se_2C nanosheets with high potential for Li-ion battery anodes. ACS Appl Nano Mater. 2025;8(43):20792–800. [CrossRef].
46. Herabad SR, Soleimani HR, Ali Mohebpour M. Novel 2D transition metal carbo-chalcogenides as anode materials: A comparative study of Sc_2S_2C and Sc_2Se_2C monolayers. J Phys Chem Solids. 2025;205:112779. [CrossRef].
47. Ahmed S, Ghani A, Bibi K, Rajput S, Zhang A. Metallic MoScP2Se6 monolayer with ultrafast ion diffusion for high-performance sodium and potassium-ion batteries. Mater Sci Semicond Process. 2026;207:110453. [CrossRef].
48. Shu Z, Cui X, Wang B, Yan H, Cai Y. Fast intercalation of lithium in semi-metallic γ-GeSe nanosheet: A new group-IV monochalcogenide for lithium-ion battery application. ChemSusChem. 2022;15(15):e202200564. [CrossRef].
49. Zhou Y, Zhao M, Chen ZW, Shi XM, Jiang Q. Potential application of 2D monolayer β-GeSe as an anode material in Na/K ion batteries. Phys Chem Chem Phys. 2018;20(48):30290–6. [CrossRef].
50. Zhang WX, He WH, Li TT, Zhao JW, He C. Theoretical prediction of germanium selenium nanosheet as a potential anode material for high-performance alkali-metal based battery. J Solid State Chem. 2019;277:17–24. [CrossRef].
51. Wang J, Wu H, Liu Z, Pan M, Huang Z, Pan L, et al. Theoretically evaluating two-dimensional tetragonal Si_2Se_2 and $SiSe_2$ nanosheets as anode materials for alkali metal-ion batteries. Phys Chem Chem Phys. 2022;24(42):26241–53. [CrossRef].
52. Zafer T, Singh D. Thermodynamic and kinetic properties of 2D carbon selenide for efficient sodium-ion batteries (SIBs). Appl Surf Sci. 2026;732:166511. [CrossRef].
53. Wang T, Yin L, Zhao R, Xia C, Zhao X, An Y, et al. First-principles study of monolayer $SnS_{2(1-x)}Se_{2x}$ alloys as anode materials for lithium ion batteries. Appl Surf Sci. 2018;457:256–63. [CrossRef].
54. Lin H, Lou N, Yang D, Jin R, Huang Y. Janus MoSSe/graphene heterostructures: Potential anodes for lithium-ion batteries. J Alloys Compd. 2021;854:157215. [CrossRef].
55. He J, Chen J, Ma S, Jiao Z. Janus $MoSSe/C_3N$ heterostructures: A flexible anode for lithium/sodium-ion batteries. Phys E Low Dimension Syst Nanostruct. 2022;144:115402. [CrossRef].
56. Zhang W, Jin X, Qu J, Liu S, Hu F, Wang X, et al. Are Janus $MoSSe/Ti_3C_2$-MXene heterostructures excellent anode materials for Na-ion batteries? A computational insight combined experiment. Appl Surf Sci. 2023;614:156196. [CrossRef].
57. Kang W, Wang Y, Cao D, Kang Z, Sun D. *In-situ* transformation into $MoSe_2/MoO_3$ heterogeneous nanostructures with enhanced electrochemical performance as anode material for sodium ion battery. J Alloys Compd. 2018;743:410–8. [CrossRef].
58. Liu M, Liu R, Xu Y, Ye Z, Liu Z, Zhang Y, et al. Designing hollow Ti_3C_2@$TiSe_2$ composites for long cycle life of sodium-ion storage. Electrochim Acta. 2024;475:143567. [CrossRef].
59. Wang K, Liu M, Huang D, Li L, Feng K, Zhao L, et al. Rapid thermal deposited GeSe nanowires as a promising anode material for lithium-ion and sodium-ion batteries. J Colloid Interface Sci. 2020;571:387–97. [CrossRef].
60. Lu S, Luo W, Chao Z, Liu Y, Zhang Z, Fan J. New type of SnSe/CoSe@C anode for lithium-ion batteries. Energy Fuels. 2022;36(4):2260–7. [CrossRef].